THE JOURNAL OF PHYSICAL CHEMISTRY A

ARTICLE

pubs.acs.org/JPCA

Excited State Relaxation Dynamics of Model Green Fluorescent Protein Chromophore Analogs: Evidence for *Cis*−*Trans* Isomerism

Shahnawaz Rafiq,[†] Basanta Kumar Rajbongshi,[†] Nisanth N. Nair, Pratik Sen,* and Gurunath Ramanathan*

Department of Chemistry, Indian Institute of Technology Kanpur, Kanpur, 208 016, UP, India

Supporting Information

ABSTRACT: Two green fluorescent protein (GFP) chromophore analogs (4*Z*)-4-(*N*,*N*-dimethylaminobenzylidene)-1-methyl-2-phenyl-1,4-dihydro-5*H*-imidazolin-5-one (DMPI) and (4*Z*)-4-(*N*,*N*-diphenylaminobenzylidene)-1-methyl-2-phenyl-1,4-dihydro-5*H*-imidazolin-5-one (DPMPI) were investigated using femtosecond fluorescence up-conversion spectroscopy and quantum chemical calculations with the results being substantiated by HPLC and NMR measurements. The femtosecond fluorescence transients are found to be biexponential in nature and the time constants exhibit a significant dependence on solvent viscosity and polarity. A multicoordinate relaxation mechanism is proposed for the excited state relaxation behavior of the model GFP analogs. The first time component (τ_1) was assigned to the formation of twisted intramolecular charge transfer (TICT) state along the rotational coordinate of N-substituted amine group. Time resolved intensity normalized and area normalized emission spectra (TRES and TRANES) were constructed to authenticate the occurrence of TICT state in subpicosecond time scale. Another picosecond time component (τ_2) was attributed to internal conversion via large amplitude motion along the exomethylenic double bond which has been enunciated by quantum chemical calculations. Quantum chemical calculation also forbids the involvement of hula-twist because of high activation barrier of twisting. HPLC profiles and proton-NMR measurements of the irradiated analogs confirm the presence of *Z* and *E* isomers, whose possibility of formation can be accomplished only by the rotation along the exomethylenic double bond. The present observations can be extended to *p*-HBDI in order to understand the role of protein scaffold in reducing the nonradiative pathways, leading to highly luminescent nature of GFP.

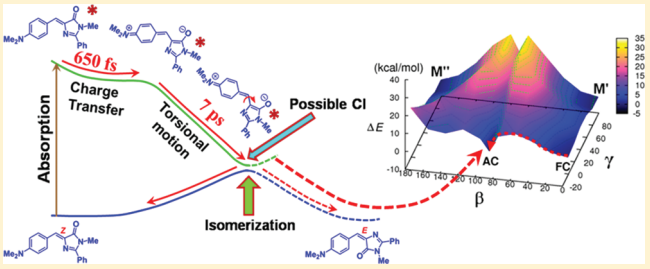

1. INTRODUCTION

The green fluorescent protein (GFP) of the jellyfish *Aequorea victoria* is very widely used as a genetically encoded noninvasive fluorescence marker in bioimaging.[1] Some years after its discovery, it was shown that GFP could be cloned and expressed in other organisms.[1,2] The utility of GFP as a fluorescence marker gained all around acceptance especially after the beautiful fluorescence images obtained by Chalfie et al.[1] Advanced developments predominantly through mutagenesis to increase the stability and diversify the spectral range enhanced the vast potential of GFP and other fluorescent proteins.[3−5] This protein is particularly useful due to its stability and the fact that its chromophore is generated in situ by an autocatalytic post-translational cyclization that does not require a cofactor.[6] GFP's meteoric rise as a molecular imaging tool took place after Roger Tsien's group developed GFP variants with much improved biological and photophysical properties, as well as additional color variants with distinctive emissions ranging from blue and cyan to yellow.[7−10] The chromophore responsible for the fluorescence of this protein is *p*-hydroxybenzylideneimidazolinone (*p*-HBDI). The fluorescence arises from both its neutral and anionic forms, which is generated upon ultrafast excited state intramolecular proton transfer in the neutral form.[11,12] One intriguing feature about the wild type green fluorescent protein (*wt*GFP) is that while the chromophore in its intact protein has a quantum yield of ∼0.8 and an excited state lifetime of 3.3 ns,[13,14] its isolated chromophore *p*-HBDI has a quantum yield that is almost 4000-fold less and a lifetime around 3300-fold less than the *wt*GFP.[15] Further, the denatured protein, isolated fragments of protein containing the chromophore, and most of the synthetic model compounds of the GFP chromophore, are all weakly fluorescent ($\phi \approx 10^{-3}$) in bulk solutions at standard conditions.[15,16] These observations have led to an extensive investigation of the photophysical properties of GFP and its mutants,[17] the synthetic derivatives of the GFP chromophore and its related model systems, by theory and experiment.[14−16,18−26] The majority of the literature suggest that HBDI and its analogs undergo excited state twisting that triggers internal conversion (IC) making them weakly fluorescent.[18−25] Such weak fluorescence is essentially a characteristic feature of flexible chromophores like triphenylmethane (TPM) dyes, for which a large amplitude motion of phenyl rings is the main route of internal conversion.[23,27] The mechanism of IC in *p*-HBDI has long been of the subject of debate. While some suggest a single bond rotation,[18] others suggest double bond rotation[15,16,19] or a simultaneous and concerted rotation of both single and double bonds known as the hula-twist.[20] Weber et al.[21] suggest

Received: July 17, 2011
Revised: October 13, 2011
Published: October 13, 2011

Scheme 1. Two GFP Chromophore Analogs DMPI and DPMPI along with the Main GFP Chromophore *p*-HBDI[a]

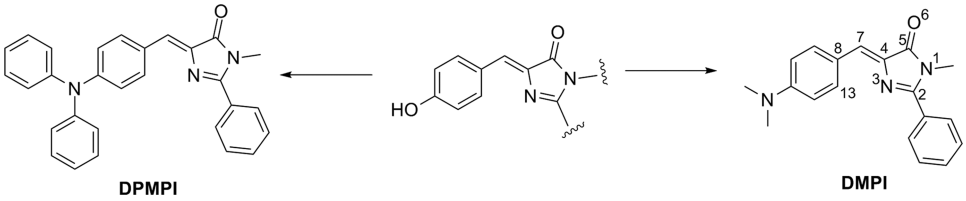

[a] The *p*-HBDI analog studied extensively by others is the analog in the middle where the wiggly lines representing protein chains are now only methyl groups. Same atom labels are used for all analogs.

a possibility of double bond rotation and a hula-twist in the neutral chromophore, whereas Baldridge et al.[22f] suggested IC by twisting of the exomethylene double bond in their alkyl substituted analogs in octaacid cavitand, while in solution phase, the IC was by a combination of one bond flip and twisting of the bridging single bond.[24] Usman et al.[25] performed ultrafast polarization sensitive infrared (IR) spectroscopic studies on *p*-HBDI. They suggested that both hula-twist and rotation around the exomethylene double bond can lead to IC. While the double bond rotation or hula-twist is accepted as the twisting motion that triggers IC, mechanistic explanations of these energetically uphill processes are not yet available. Since *cis*−*trans* isomerization is an obvious outcome of double bond rotation and hula-twist, both isomers should be detectable at the end of any photoirradiation.

To furnish a deeper understanding of the mechanism of IC, we designed and synthesized two new analogs of HBDI that differ in the bulkiness of the electron donor substituent with considerable design inputs from studies by earlier workers on dimethylamino group containing fluorophores such as the dansyl group.[28] The other analog was designed to increase the bulkiness and thus act as a reporter for large amplitude motion. Fluorescence up-conversion studies and quantum chemical calculations were performed to understand the excited state relaxation mechanism of the analogs under consideration. The present study was undertaken to reveal the nonradiative pathways operational in GFP chromophore analogs.

2. EXPERIMENTAL SECTION

2.1. Synthesis of GFP Chromophore Analogs. The molecules (Scheme 1) were synthesized using previously published procedures[29−33] (see Supporting Information). The two compounds were fully characterized by ^{1}H NMR, ^{13}C NMR and Mass (available in Supporting Information, Figures S1−S4).

2.2. Steady State Measurements. Steady state absorption spectra and fluorescence spectra were measured using a commercial UV−vis spectrophotometer (JASCO V-550) and fluorimeter (Fluorolog 3-21, Horiba Jobin-Yvon), respectively. All measurements have been done at 22 °C.

2.3. Femtosecond Fluorescence Up-conversion Measurements. The fluorescence transients were measured in a femtosecond fluorescence up-conversion setup (FOG-100, CDP Corp.). The details of this setup are discussed elsewhere.[34] Briefly, the sample was excited at 435 nm using the second harmonic of a mode-locked Ti-sapphire laser (Tsunami, Spectra Physics), pumped by a 5 W Millennia (Spectra Physics). To generate the second harmonic, we used a nonlinear crystal (1 mm β barium borate, θ = 25°, ϕ = 90°). The fluorescence emitted from the sample was up-converted in another nonlinear crystal (0.5 mm β barium borate, θ = 38°, ϕ = 90°) by using the fundamental beam as a gate pulse. The up-converted light was dispersed in a monochromator and detected by photon counting electronics. A cross-correlation function obtained with the use of Raman scattering from water displayed a full width at half-maximum (fwhm) of 350 fs. Femtosecond up-conversion measurements were performed for both the molecules in various glycerol-methanol mixtures of different viscosities and also in a number of isoviscous solvents of different polarities. The decays were deconvoluted using a Gaussian shape for the exciting pulse using commercial software (IGOR Pro, WaveMetrics). The up-conversion decay transients were measured at their emission maxima, unless otherwise mentioned. All measurements reported here were made at 20 °C.

2.4. Irradiation Experiment and HPLC Analysis. A solution of DMPI in acetonitrile was irradiated at 467 nm (absorption at 467 nm ≈ 1.54) using a xenon arc lamp (450 W, 18 V, 25 A, Ushio code UXL-450S−O) in a spectrofluorimeter (Fluorolog 3-21, Horiba Jobin-Yvon) with an excitation slit of 10.0 nm for 11 h. This solution was then injected in an analytical HPLC (Amersham Biosciences, P-900, C-18 reverse phase column, 150 × 46 mm, kromasil 700C-18, particle size 5 μm) and compared with the chromatograms obtained before irradiation. An isocratic solvent of 65% methanol in water was used as the eluent and the flow rate was kept at 1.0 mL/min. In a separate experiment, DMPI (8.0 mg) was dissolved in deutero-chloroform and its ^{1}H NMR was recorded in a 400 MHz NMR spectrometer. The solution in the NMR tube was irradiated similarly using an excitation slit 5.0 nm for 16 h. Its ^{1}H NMR was recorded in a 400 (400 MHz) JEOL NMR spectrometer and ^{13}C NMR was recorded in a 500 (125 MHz) JEOL NMR spectrometer.

3. THEORETICAL CALCULATIONS

Computation of the first singlet excited state (S1) potential energy surface of DMPI molecule was done by time-dependent density functional theory (TDDFT)[35] as implemented in the Gaussian03 software package.[36] For all TDDFT calculations 20 excited states were included and were done employing 6-31G** basis set and B3LYP[37] density functional. The potential energy surface (PES) corresponding to the electronic ground state (S0) was computed using the density functional theory (DFT) at the same level. The three-dimensional potential energy surface was constructed along the dihedral angles γ (C4−C7−C8−C13) and β(N3−C4−C7−C8) for S_0 and S_1 states. PES of the ground state and the first excited state were computed by varying dihedral angle γ(C4−C7−C8−C13) between −2° to 98° in

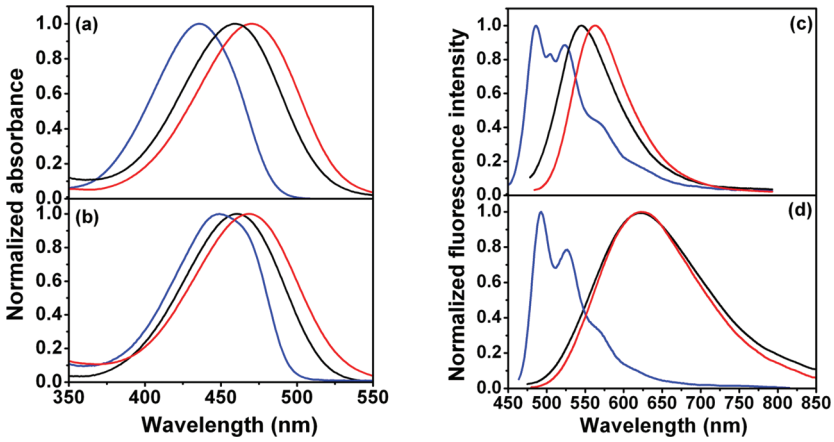

Figure 1. Steady state absorption of the two synthetic GFP chromophore analogs; (a) DMPI and (b) DPMPI in three different solvents: (1) Cyclohexane (blue line); (2) Methanol (black line); and (3) 50% gylcerol−methanol mixture (red line). Steady state fluorescence spectra of (c) DMPI and (d) DPMPI in three different solvents: (1) Cyclohexane (blue line); (2) Methanol (black line); and (3) 50% gylcerol−methanol mixture (red line).

20° increments, and β(N3−C4−C7−C8) from 0° to 180° by 20° increments, including 90°, keeping all of the other degrees of freedom frozen at the X-ray structure. Thus, a total of 66 ground state and excited state calculations were performed. Calculations have been performed in vacuum as well as in acetonitrile medium (using polarizable continuum model, PCM). Since the excited state of the molecule has charge transfer character, the potential energy barriers computed using TDDFT at the S_1 excited state may have quantitative errors.[38] Thus, results of TDDFT will only be used here for obtaining a qualitative picture of the excited state dynamics. Much accurate coupled cluster methods are highly computationally demanding for the computation of the entire potential energy surface.[39]

4. RESULTS AND DISCUSSION

4.1. Steady State Absorption and Emission. The UV−vis absorption spectra of both synthetic GFP chromophore analogs (DMPI and DPMPI) are characterized by the presence of a single $S_1 \leftarrow S_0$ absorption band having a maximum located between 430 and 480 nm in a range of solvents as shown in Figure 1 (left panel). All the absorption spectra have a similar shape, and the position of the maximum depends on the nature of the substituent groups, polarity of the solvent and on the extent of hydrogen bonding. The absorption maximum of DMPI is found to be 460 and 470 nm in 0% to 50% glycerol in methanol, respectively. This bathochromic shift is assigned to the increase in polarity with increasing proportion of glycerol. Similarly for DPMPI, the shift in absorption maximum occurs from 460 to 469 nm with increase in glycerol proportion from 0% to 50%. The absorption maximum of DMPI shifts from 435 nm in cyclohexane to 460 nm in methanol. Similarly, DPMPI exhibits a shift in absorption maximum from 449 nm (in cyclohexane) to 460 (in methanol). Further, there is a significant bathochromic shift as we go from DMPI to DPMPI probably due to enhanced conjugation.

The fluorescence spectra shown in Figure 1 (right panel) of both molecules are characterized by a significant Stokes shift relative to the absorption spectra. The fluorescence intensity of both molecules shows a strong dependence on solvent viscosity and increases monotonically with an increase in the solvent viscosity. Such behavior in these analogs is quite different compared to *p*-HBDI.[22e] The emission maximum of DMPI in methanol is at 533 nm with fluorescence quantum yield of 0.002. In 50% glycerol−methanol mixture, the emission maximum of DMPI is red-shifted to 549 nm with a 13-fold increase in fluorescence quantum yield (Φ = 0.026). For DPMPI, there is almost no shift in the emission maximum from methanol (622 nm) to 50% glycerol−methanol (623 nm) because the extended conjugation causes an increase in electron density in the σ bond between the *N*,*N*-diphenylamine moiety and the phenyl ring, which renders the former moiety rigid. Both DMPI and DPMPI also show substantial polarity dependence in their emission spectra. In DMPI, the emission shows moderate bathochromic shift from cyclohexane (482 nm) to methanol (533 nm) and 50% glycerol−methanol (549 nm), while in DPMPI, there is large bathochromic shift from cyclohexane (493 nm) to methanol (622 nm). The observed solvatochromism in our analogs is different from that exhibited by *p*-HBDI.[22e] In cyclohexane, a prominent vibrational structure is observed for both molecules. As the solvent polarity increases, the vibrational structure vanishes, and the emission maximum shifts to longer wavelengths. In methanol, DMPI has an emission maximum at 533 nm and DPMPI is characterized by the maximum at 622 nm.

4.2. Femtosecond Fluorescence Up-Conversion Study. *4.2.1. Effect of Viscosity on Excited State Relaxation Dynamics.* The fluorescence transients of both synthetic analogs in various glycerol−methanol mixtures were measured at their respective emission maximum and are shown in Figure 2. The logarithmic plots are shown in Figure S5a of Supporting Information. The decay traces were fitted by a sum of two exponentials and the resulting time constants are shown in Table1. For DMPI, in pure methanol, the two time constants are τ_1 = 590 fs and τ_2 = 4.3 ps. As we increase the proportion of glycerol from 0% to 50% glycerol in methanol, τ_1 increases to 1.1 ps and τ_2 to 10 ps. For DPMPI, τ_1 increases from 7.9 to 17.3 ps and τ_2 from 37.7 to 81 ps with increase in viscosity from pure methanol to 50% glycerol−methanol mixture. The viscosity dependence of the nonradiative decay pathway is often described in terms of following the power law empirical relationship.[27]

$$\tau_{nr} = \eta^{\alpha} \quad (1)$$

Where η is viscosity of the solvent and α is a factor that gives us the degree of dependence and whose value varies from 0.1 to 1.0.[27] The time constants of both DMPI and DPMPI were

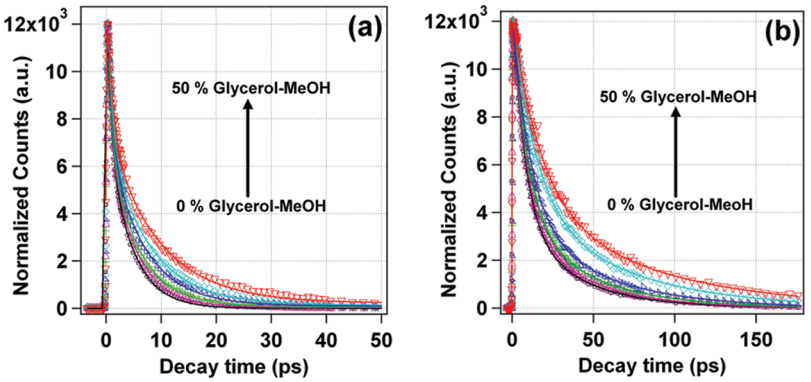

Figure 2. Femtosecond fluorescence up-conversion transients of (a) DMPI and (b) DPMPI in different glycerol−methanol mixtures with varying viscosity. As the viscosity of the medium increases, the decay becomes slower in both cases.

Table 1. Time Constants τ_1 and τ_2 of Two Synthetic Analogs, DMPI and DPMPI Tabulated As a Function of Viscosity of Glycerol−Methanol Mixtures

glycerol in methanol		DMPI		DPMPI	
percentage	viscosity (cP)	τ_1 (ps)	τ_2 (ps)	τ_1 (ps)	τ_2 (ps)
0	0.543	0.59	4.3	7.9	37.7
10	1.145	0.65	4.8	8.2	40.2
20	2.415	0.67	5.4	9.6	46.5
30	5.093	0.86	6.7	11.1	52.7
40	10.741	0.86	7.7	14.1	65.5
50	22.651	1.10	10.0	17.3	81.0

plotted against the viscosity of the solvent (See Supporting Information, Figure S6). In both molecules, the τ_1 and τ_2 increase with an increase in solvent viscosity. For DMPI, τ_1 and τ_2 follow power law viscosity dependence with α values of 0.51 and 0.46, respectively. While for DPMPI, the α value for the two time constants is 0.51. The dependence of τ_1 and τ_2 time constants on the microviscosity of glycerol−methanol mixtures suggests the involvement of a large amplitude motion in their excited state relaxation dynamics. The relative comparison of the time constants of these molecules furnishes information about the effect of substitution on the excited state dynamics of these molecules. In pure methanol, as we go from DMPI to DPMPI, wherein the two methyl groups on nitrogen have been substituted by two bulky phenyl groups, there is a substantial increase in magnitude of time constants. While the faster time component τ_1 increases from 590 fs to 7.9 ps, the slower time component τ_2 increases from 4.3 to 37 ps. The increase in magnitude of time constants can be ascribed mainly to the increased conjugation and also the frictional resistance offered by solvent molecules to the torsional motion of the *N*,*N*-diphenylamine moiety.

Previously it has been proposed by many authors, that "hula-twist", a volume conserving torsional motion of the rings about the bridging bond is responsible for the excited state relaxation of GFP chromophore and its analogs.[10,11,23] The experimental observation of the analogs considered in this work does not support the involvement of hula-twist as a primary relaxation coordinate, because of the evidence of large amplitude motion. On the basis of the low quantum yield of DMPI in nonviscous solvents (quantum yields of DMPI in cyclohexane, ethyl acetate, acetonitrile, and methanol are, respectively, 0.006, 0.005, 0.003, and 0.002), observed increase in quantum yield with increase in viscosity, and viscosity dependent lifetime, we assign the long time component (τ_2) to the decay of S_1 to S_0 state by internal conversion via a large amplitude motion.[16−21] Weber et al.[21] showed the major and dominant relaxation pathway in zwitterionic *p*-HBDI is the large amplitude motion of benzene ring. If the excited state of DMPI involves a charge transfer coordinate, then the molecule will be zwitterionic in nature and hence the involvement of the large amplitude motion of the substituted phenyl ring may have a part to play.

4.2.2. Iso-Viscosity Analysis. Fluorescence transients of DMPI and DPMPI were measured in four polar aprotic solvents of similar viscosity but different polarities at their respective emission maximum. The decay transients are shown in Figure 3 (logarithmic plots are shown in Figure S5b of the Supporting Information) and the fitting parameters are tabulated in Table 2. In all of the solvents, the immediately formed Franck−Condon (FC) state relaxes within a time scale of a few hundred femtoseconds to an intermediate state followed by relaxation to the ground state through internal conversion on a time scale of sub-hundred picoseconds. For DMPI, in cyclohexane (λ_{em} = 482 nm), time constant τ_1 is 850 fs and as we change the dielectric media from cyclohexane ($\varepsilon = 2$) to acetonitrile ($\varepsilon = 35$), τ_1 decreases to 650 fs, while the dependence of τ_2 is not monotonous. The dependence of time constant τ_1 on the polarity of the solvent implies the decay of the FC state to a relatively relaxed state, whose stability is a function of solvent polarity. As the solvent polarity increases, the solvent molecules stabilize that state in such a way that the rate of depletion of the FC state increases, leading to a faster time constant. This is possible only if that state has a charge transfer character and will be more stable in more polar solvents. It is worth mentioning that this time constant also depends on solvent viscosity and on the extent of substitution (ca. DMPI vs DPMPI).

These observations indicate the involvement of amplitude motion in the system, during the transfer of charge between donor and acceptor moiety. In order to justify the viscosity dependence of both the time constants, we propose a multicoordinate relaxation mechanism of the excited state. Upon photoexcitation, the locally excited (LE) state depletes to the charge transfer (CT) state via the rotational motion of N-substituted amine moiety attached to the phenyl ring. This provides rigidity to the σ bond between the amine group and the phenyl ring and hence the charge transfer time constant is prone to the

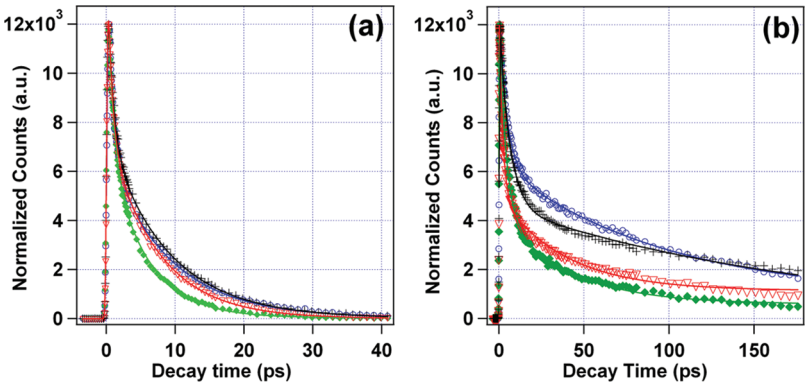

Figure 3. Femtosecond fluorescence up-conversion transients of (a) DMPI and (b) DPMPI in four isoviscous, aprotic solvents having different values of dielectric constant; cyclohexane (blue ○), chloroform (green ♦), acetone (black +), and acetonitrile (red ▽).

Table 2. Polarity Dependence of Time Constants τ_1 and τ_2 of DMPI and DPMPI in Four Isoviscous, Aprotic Solvents (Cyclohexane, Chloroform, Acetone, and Acetonitrile) of Different Dielectric Constants[a]

solvent details			DMPI		DPMPI	
solvent	viscosity (cP)	dielectric constant	τ_1 (fs)	τ_2 (ps)	τ_1 (ps)	τ_2 (ps)
cyclohexane	0.89	2.00	850 (0.53)	8.8 (0.47)	4.6 (0.52)	96 (0.48)
chloroform	0.54	4.72	810 (0.51)	5.5 (0.49)	3.9 (0.68)	39 (0.32)
acetone	0.30	20.56	790 (0.48)	8.7 (0.52)	5.1 (0.68)	61 (0.32)
acetonitrile	0.341	35.95	650 (0.50)	7.2 (0.50)	2.0 (0.69)	75 (0.31)
methanol	0.543	32.63	590 (0.50)	4.3 (0.50)	7.9 (0.70)	37 (0.30)
ethanol	1.087	24.35	730 (0.55)	6.3 (0.45)	9.1 (0.55)	57 (0.45)
n-butanol	2.61	17.43	800 (0.55)	6.4 (0.45)	10.7 (0.4)	85 (0.60)

[a] The other three solvents (methanol, ethanol, and *n*-butanol) depict the dependence of time constants on the hydrogen bond donating capability of solvents. The parameters in parentheses represent the amplitude of the respective time constants.

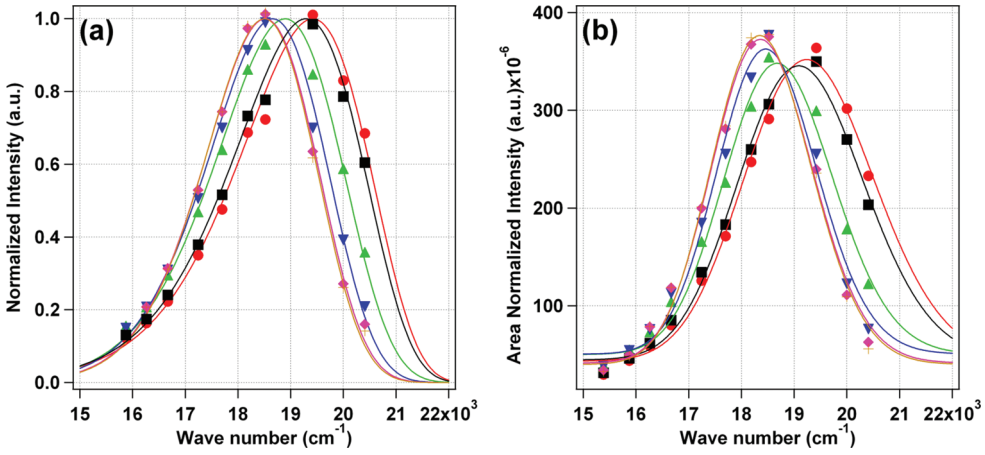

Figure 4. (a)Intensity normalized time-resolved emission spectra (TRES) of DMPI in acetonitrile, constructed from the decay transients obtained at ten different wavelengths. The time-resolved emission spectra were plotted for 0 ps (red ●), 0.1 ps (black, ■), 0.5 ps (green, ▲), 1 ps (blue,▼), 3 ps (pink, ♦) and 5 ps (orange, +). (b) Time-resolved area normalized emission spectra (TRANES) of DMPI in acetonitrile. The symbols have their usual meaning as mentioned for TRES. The TRANES reports the occurrence of an isoemissive point and hence implies the existence of two states in the excited state deactivation process.

viscosity of the medium. The involvement of the torsional motion of N-substituted amine moiety also explains the large magnitude of the CT time component in DPMPI than DMPI. Subsequently, the CT state relaxes via conical intersection to the ground state along the torsional motion of N-substituted phenylamine moiety about the exomethylenic double bond, paving the path for the *cis*−*trans* isomerization.

4.2.3. TRES and TRANES Measurements. Fluorescence up-conversion transients of DMPI in acetonitrile were recorded at eleven different wavelengths throughout the emission

dx.doi.org/10.1021/jp206815t |*J. Phys. Chem. A* 2011, 115, 13733–13742

spectrum with the relaxation dynamics exhibiting substantial emission wavelength dependence. As already mentioned, the excited state relaxation of DMPI involves two time constants. The faster time constant can be the solvent relaxation or any other excited state reaction like intramolecular charge transfer, while the longer time constant corresponds to the internal conversion via large amplitude motion from S_1 to S_0 potential energy surface. The time-resolved intensity normalized and area normalized emission spectra (TRES and TRANES) were constructed using the parameters of best fit to the fluorescence decays and the steady state emission spectra.[40,41] Figure 4a shows the intensity normalized time-resolved emission spectra (TRES) of DMPI constructed at six times viz., 0, 0.1, 0.5, 1, 3, and 5 ps. There is a continuous shift in the wavenumber corresponding to maximum intensity up to 5 ps, which marks the limit of any depletion of LE state and formation of CT state, with an overall Stokes shift of 1000 cm^{-1}. Constructed TRANES (Figure 4b) is characterized by the presence of an iso-emissive point representing the equilibrium between the two states viz., locally excited FC state on the higher wavenumber side and charge transfer CT state on the lower wavenumber state. As the time evolves from 0 to 5 ps, the intensity of the LE state decreases and that of the CT state increases, after which there is practically no change in the intensity of either of the states. The occurrence of a single iso-emissive point in the TRANES of DMPI suggests a two state decay kinetics representing the dielectric dependent decay of LE state to CT state within 3−5 ps, followed by the depletion of TICT state to the ground state through internal conversion via large amplitude motion.

4.2.4. Effect of Intermolecular Hydrogen Bonding on Relaxation Behavior. Intermolecular hydrogen bonding is one of the significant nonradiative decay pathways of the S_1 state in a large number of chromophores especially containing a hydrogen bond donor or acceptor group. We measured the fluorescence transients of both the synthetic analogs in alcoholic solutions of different hydrogen bond donating capabilities, but with almost similar viscosities and polarities. In methanol, for DMPI, the CT time constant τ_1 = 590 fs and IC time constant τ_2 = 4.3 ps. Going down to *n*-butanol in the series, τ_1 increased to 807 fs and τ_2 incremented to 6.4 ps (Table 2). A similar type of increase is observed for DPMPI. The more viscous nature of higher order alcohols can also induce an increase in the magnitude of the time constants. However, after subtracting the viscosity effect from the experimentally obtained parameters, the time constants are found to depend on the H-bonding ability of the solvents as well. The reason is ascribed to the presence of intermolecular hydrogen bonding between solvent molecules and the chromophore.

Similar hydrogen bonding dependent dynamics have also been proposed by Vauthey and co-workers,[23] wherein the charge transfer results in an increase of electron density on the carbonyl group for other GFP chromophore analogs. This enhances the acidity of amino group and the basicity of carbonyl group, which in turn leads to an enhancement of hydrogen bonding ability in the excited state.[42−44] The stretching vibrational modes of the hydrogen bonds act as a sink for the $S_1 \rightarrow S_0$ nonradiative decay and thus in this way the electronic energy gets dissipated among the vibrational modes of the hydrogen bonds.[23] The increase of hydrogen bonding ability while going up from *n*-butanol to methanol induces stronger intermolecular hydrogen bonding interactions, which leads to an acceleration of the S_1 state decay and consequently a decrease of time constants. A similar conclusion is reached in the case of methanol and acetonitrile. Both solvents have almost similar viscosities and dielectric properties, but differ in their hydrogen bond donating abilities (methanol is a more efficient hydrogen bond donor than acetonitrile). The S_1 relaxation time constant (τ_2) of DMPI decreases from 7.2 ps in acetonitrile to 4.3 ps in methanol, which is a direct consequence of intermolecular hydrogen bonding. The similar gradation is observed for DPMPI as well.

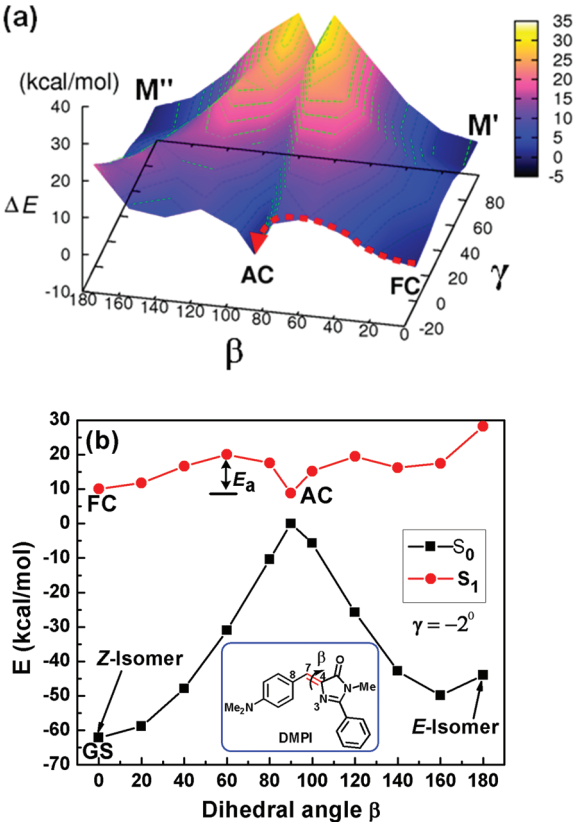

Figure 5. (a) Calculated three dimensional potential energy surface of the S_1 state of DMPI as a function of dihedral angles β and γ. The S_0 surface is dropped for clarity of the picture. (b) Energy profiles of the S_0 and S_1 states as a function of β (rotation about C4−C7 double bond), keeping γ fixed at −2°.

The results of steady state fluorescence and femtosecond up-conversion measurements comprehend the viscosity-dependent decay of the excited state. The strong viscosity dependence suggests a large amplitude motion of some bulky groups playing a role in the internal conversion process. For some GFP chromophore analogs, it has already been proposed that torsional motion along the exomethylene double bond[15,16,19] is the primary relaxation coordinate for internal conversion, which motivated us to look for the nonradiative decay channel responsible for the depletion of the excited state by theoretical calculations.

4.3. Potential Energy Surface (PES) Calculations. The potential energy surfaces of the S_0 and S_1 states of DMPI were calculated in vacuum and are shown in Figure 5. These surfaces are observed to form a "conical intersection"[16,19c,45] when β is 90°, and the coordinates representing the point are (γ,β) = (−2°,90°) labeled by **AC** in Figure 5a. At the dihedral angles of ground state optimal values $[(\gamma,\beta) = (-2°,0°)]$ is a local minimum (**FC**) on the S_1 surface. The dihedral angles (γ,β) = (90°,0°) and (90°,180°) represent two other minimum energy

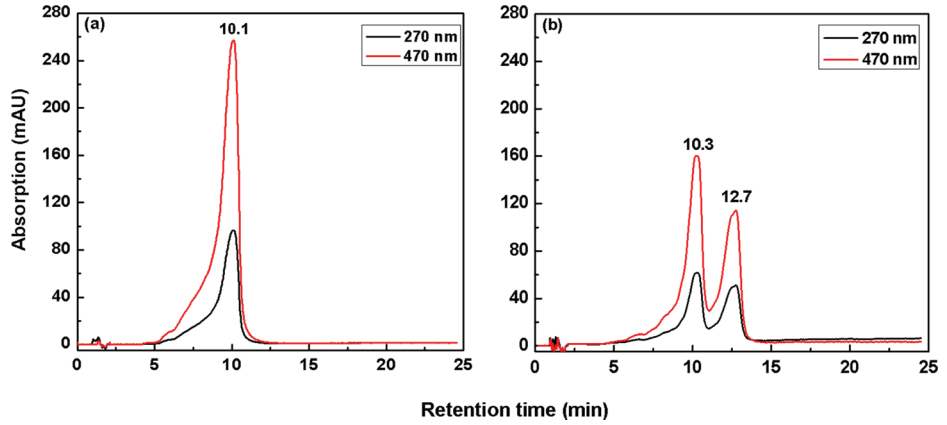

Figure 6. HPLC chromatograms of DMPI (a) before and (b) after irradiation at 467 nm for 11 h in acetonitrile. An isocratic 65% methanol in water was used as the eluent on a C-18 reverse phase analytical column with a flow rate 1 mL/min.

structures on the S_1 surface (labeled **M′** and **M″**, respectively), and are nearly degenerate with **FC** with an energy difference of only 0.25 kcal/mol. The potential energy barrier along the minimum energy pathway (MEP) for **FC** → **AC** transition, as indicated by the dotted lines in Figure 5a, is about 10 kcal/mol (see also Figure 5b). Most interestingly, the MEP has no change along the γ coordinate, aligned parallel to the β coordinate axis. The position of the transition state along the MEP is at $\beta = 60°$. The forward and reverse barrier separating **FC** and **M′** is estimated to be less than a kT at room temperature. However the gap between the S_0 and S_1 states is too large (57.7 kcal/mol) to provide coupling between these two states (Figure S7a, Supporting Information), for which it appears that rotation along the C7−C8 single bond cannot lead to internal conversion. The minimum **M″** is kinetically inaccessible due to large potential energy barriers separating **FC**/**M′** and **M″**. Since the S_1 potential energy approaches the S_0 surface and forms a conical intersection at $\beta = 90°$, one may expect *Z*-*E* isomerization about the exomethylene double bond (C4−C7) of DMPI. The S_0 surface reveals that the *E*-isomer is 11 kcal/mol less stable than the *Z*-isomer (Figure 5b).

The excited state charge transfer in the molecule introduces a partial double bond character to the C7−C8 bond, thus the barrier going from **M′** to **M″** is expected to be much larger than that estimated by TDDFT calculations (see Supporting Information Figure S7b). We believe that this is the result of the artifact of TDDFT in describing the charge-transfer at the excited states while employing the ground state density functionals. It is known that the excitation energy is underestimated by TDDFT in such cases.[38] The results of the theoretical calculations alone seem to contradict the internal conversion by the single bond rotation involving the phenyl ring in the model systems of HBDI, as suggested by many authors[18] including us. Overall, this strongly suggests IC by rotation along the exomethylene double bond (C4−C7) as the main relaxation coordinate. This also clearly rules out a "hula twist" mechanism for internal conversion in these molecules. Voityuk and co-workers[19c] found a 3.2 kcal/mol energy barrier for the double-bond rotation in the cation and a 15 kcal/mol energy gap for the double-bond rotation in the anion of a model system of HBDI, leading them to propose that IC is indeed possible in both cases. We also have calculated the S_0 and S_1 potential energy surfaces using polarizable continuum model (PCM) with acetonitrile as a solvent. Incorporation of the implicit solvent effect does not alter the main conclusions derived in vacuo (see Figure S8, Supporting Information).

4.4. HPLC and NMR Analysis. HPLC chromatograms of *Z*-DMPI at 270 and 470 nm obtained from a solution in acetonitrile show one absorption peak at 10.1 min (Figure 6a). This solution was irradiated at 467 nm by a xenon short arc lamp (450 W) for 11 h. HPLC chromatograms at 270 and 470 nm of this irradiated solution show two close but separated peaks at 10.3 and 12.7 min (Figure 6b) with approximate area of 60% and 40%, respectively. This observation suggests isomerization about the exomethylene double bond and suggests the presence of *Z*-DMPI (60%) and *E*-DMPI (40%) in the solution. Further evidence of isomerization about the exomethylene double bond was obtained from analysis of ^{1}H and ^{13}C NMR of the irradiated sample.

Before irradiation, ^{1}H NMR of a solution of *Z*-DMPI in deutero-chloroform shows all of the protons (Figure 7a)—two singlets from the methylamine and dimethylamine protons, one aromatic doublet from the Ha protons, one olefinic singlet from the Hc proton, two aromatic multiplets from the Hd, He, and Hf protons and one aromatic doublet from the Hb protons. On the basis of the integration of protons and coupling constants in ^{1}H NMR, ^{13}C NMR chemical shifts, (Figure S3 and S9, Supporting Information), and crystal structure,[29] DMPI has been authenticated as a single compound, with *Z*-configuration. After irradiation, each of the above signals is appearing as doublet except the N-methyl group singlet (Figure 7b). The appearance of the dual signals is better understood from the integrations of the signals (Figure S10, Supporting Information). Although the N-methyl group is giving only one singlet, its integration is equivalent to five protons (Figure S10, Supporting Information), indicating overlap of two N-methyl groups of two isomeric *Z*-DMPI and *E*-DMPI. A new aromatic doublet from the Hb′ protons is shifted further downfield because of the possibility of formation of an intramolecular hydrogen bond with the carbonyl oxygen atom.[29] A new olefinic singlet from the Hc′ proton is also observed downfield. The ratio of the integrations of the Hb′ protons to Hb protons or He′ protons to He protons or Hc′ protons to Hc protons shows isomerization of 43% *Z*-DMPI to *E*-DMPI. The ^{13}C NMR shows the presence of all of the equivalent carbon atoms (Figure S11, Supporting Information) of two isomeric DMPI.

The experimental observation of the existence of *Z*- and *E*-isomers on irradiation and the existence of conical intersection

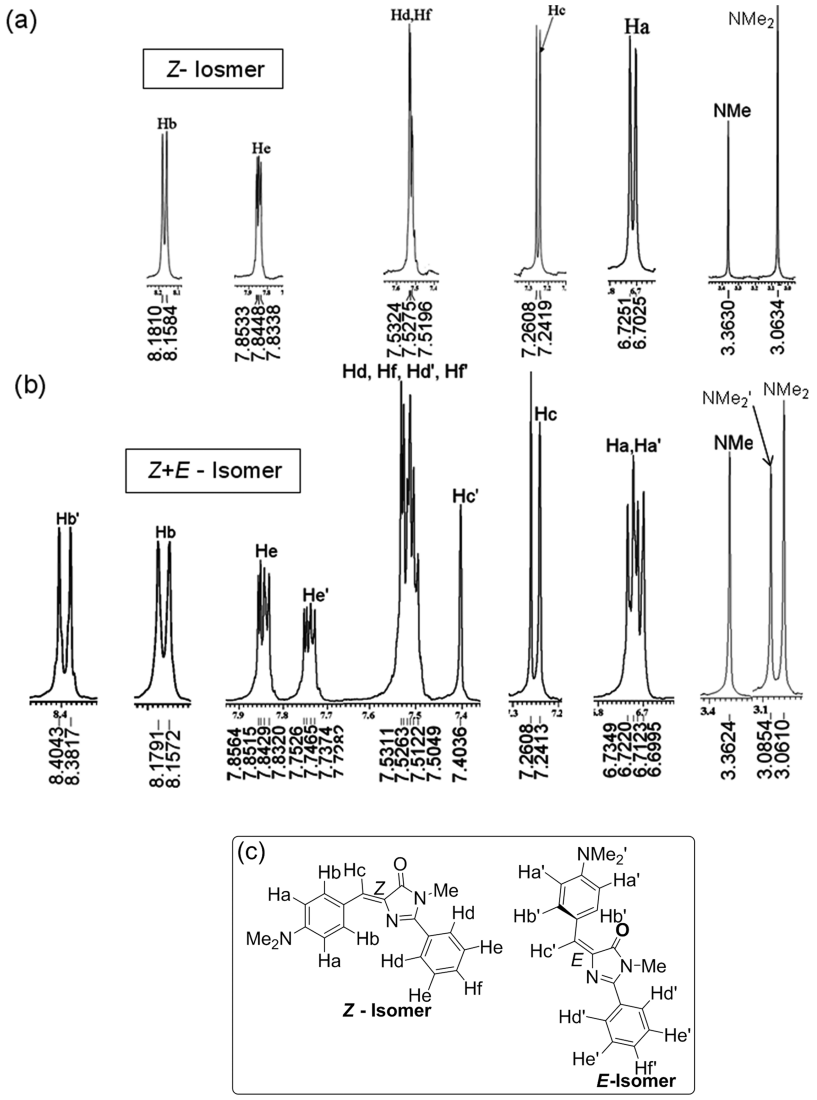

Figure 7. (a) ^{1}H NMR (400 MHz, $CDCl_3$) of *Z*-DMPI before irradiation. The signals are assigned to protons as labeled in the structures of *Z*-DMPI and *E*-DMPI shown in (c). (b) ^{1}H NMR (400 MHz, $CDCl_3$) of *Z*-DMPI and *E*-DMPI after irradiation of *Z*-DMPI in $CDCl_3$ at 467 nm for 16 h. The signals are assigned to protons as labeled in structures of *Z*-DMPI and *E*-DMPI.

Scheme 2. In DMPI, Intramolecular Charge Transfer Occurs First for Which the Exo-Methylene Double Bond (C4−C7) Becomes Predominantly a Single Bond (Right Side)[a]

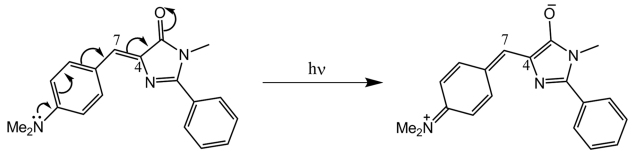

[a] After charge transfer, DMPI can now undergo rotation about the resulting C4−C7 single bond (dihedral angle β).

between the excited and the ground state substantiate the consideration of involvement of torsional motion of the exomethylenic double bond as the dominant excited state relaxation coordinate for the present analogs. The charge transfer provide rigidity to the σ bond between amine and phenyl moiety and also reduces double bond character of the exomethylenic bond (Scheme 2) leading to internal conversion via rotation about the latter bond. Furthermore, the proton at the para-position of the benzene ring attached to the 2-position of the imidazolin-5-one ring is shifted upfield as compared to the protons at the ortho- and the meta-positions, suggesting buildup of electron density at the para-position, which may be attributed to the charge transfer from the *N*,*N*-substituted amine.

The excited state dynamics of DMPI in acetonitrile can thus be summarized as shown in Scheme 3. Excitation of the *Z*-isomer forms the locally excited (LE) state which undergoes an ultrafast intramolecular charge transfer along the rotational coordinate of *N*-substituted amine on a time scale of ∼650 fs to form the twisted intramolecular charge transfer (TICT) state. The TICT state subsequently undergoes twisting with a 7 ps time component about the exomethylenic double bond (C4−C7) having a reduced double-bond character and reaches the region of conical intersection with approximately perpendicular geometry. The torsionally relaxed excited state crosses to the "hot ground state" of either of the *Z*- or *E*-isomer. The vibrationally excited ground

dx.doi.org/10.1021/jp206815t |*J. Phys. Chem. A* 2011, 115, 13733–13742

Scheme 3. Schematic Excited State Dynamics of DMPI in Acetonitrile

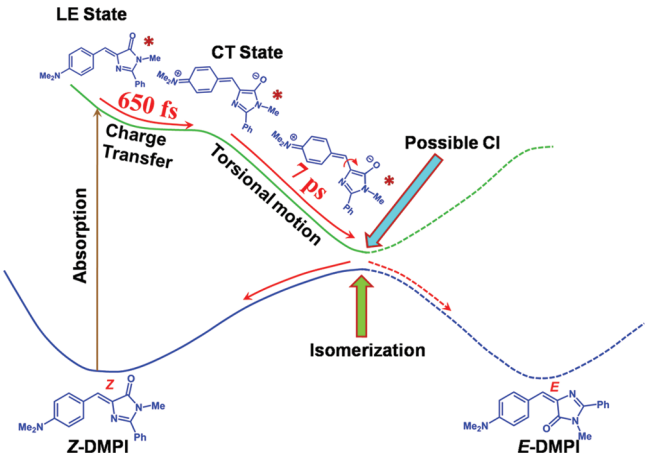

state finally relaxes to the minimum of ground state potential energy surface by thermal equilibration.

5. CONCLUSIONS

The observed solvent dependent (viz., polarity, viscosity, etc.) emission characteristics of both the analogs lead us to propose a multicoordinate excited state relaxation mechanism. The first time component is assigned to twisted intramolecular charge transfer (TICT) corresponding to the depletion of LE to CT state via the rotational motion of *N*-substituted amine group. In case of DPMPI, due to extended conjugation, the excited state charge transfer leads to more rigid σ bond between N-substituted amine and the phenyl group and hence increases the magnitude of the time constant. The TICT state then decays to the point of conical intersection via the torsional motion of N-substituted phenylamine moiety about the exomethylenic double bond as predicted by theoretical calculations. The twist about the exomethylenic double bond leads to *cis*−*trans* isomerization as evident from HPLC and ^{1}H NMR studies. The torsional motion along the single bond cannot lead to IC because of very high S_0−S_1 energy gaps, which does not allow any coupling between the two states. The TICT and IC deactivation channels make DMPI and DPMPI very weakly fluorescent. From this study, an analogy may be established between the reported analogs and *p*-HBDI to understand the role of the protein scaffold in suppressing the nonradiative pathways leading to highly fluorescent nature of wild-type GFP.

■ ASSOCIATED CONTENT

Supporting Information. Detailed synthetic procedures, NMR spectral characterization of compounds and calculated potential energy surfaces, as mentioned in the text. This material is available free of charge via the Internet at http://pubs.acs.org.

■ AUTHOR INFORMATION

Corresponding Author

*Fax: +91-512-2597436; E-mail: gurunath@iitk.ac.in (G.R.); psen@iitk.ac.in (P.S.).

Author Contributions

†These authors contributed equally to this work.

■ ACKNOWLEDGMENT

We would like to dedicate this work to our colleague Prof. N. Sathyamurthy on his 60th birthday. R.G. thanks DST and ISRO for partially supporting this research. S.R. and B.K.R. thank CSIR, India for a junior research fellowship (JRF) and senior research fellowship (SRF), respectively. We also gratefully acknowledge DST-FIST for the computational facility. We thank Professor Kankan Bhattacharyya for providing the femtosecond fluorescence up-conversion facility required for the present study under Department of Science and Technology (DST), India. This work is financially supported by the Board of Research in Nuclear Sciences (BRNS), Department of Atomic Energy, Government of India.

■ REFERENCES

(1) Chalfie, M.; Tu, Y.; Euskirchen, G.; Ward, W. W.; Prasher, D. C. *Science* **1994**, *263*, 802–805.
(2) Prasher, D.; McCann, R. O.; Cormier, M. J. *Biochem. Biophys. Res. Commun.* **1985**, *126*, 1259–1268.
(3) Tsien, R. Y. *Annu. Rev. Biochem.* **1998**, *67*, 509–544.
(4) Shaner, N. C.; Lin., M. Z.; McKeown, M. R.; Steinbach, P. A.; Hazelwood, K. L.; Davidson, M. W.; Tsien, R. Y. *Nat. Methods* **2008**, *5*, 545–551.
(5) Shaner, N. C.; Steinbach, P. A.; Tsein, R. Y. *Nat. Methods* **2005**, *2*, 905–909.
(6) Prendergast, F. G. *Methods Cell Biol.* **1998**, *58*, 1–18.
(7) Heim, R.; Cubitt, A. B.; Tsien, R. Y. *Nature* **1995**, *373*, 663–664.
(8) Heim, R.; Tsien, R. Y. *Curr. Biol.* **1996**, *6*, 178–182.
(9) Heim, R.; Prasher, D. C.; Tsien, R. Y. *Proc. Natl. Acad. Sci. U.S.A.* **1994**, *91*, 12501–12504.
(10) Ormö, M.; Cubitt, A. B.; Kallio, K.; Gross, L. A.; Tsein, R. Y.; Remington, S. J. *Science* **1996**, *273*, 1392–1395.
(11) Chattoraj, M.; King, B. A.; Bublitz, G. U.; Boxer, S. G. *Proc. Natl. Acad. Sci. U.S.A.* **1996**, *93*, 8362–8367.
(12) Brejc, K.; Sixma, T. K.; Kitts, P. A.; Kain, S. R.; Tsien, R. Y.; Ormö, M.; Remington, S. J. *Proc. Natl. Acad. Sci. U.S.A.* **1997**, *94*, 2306–2311.
(13) Meech, S. R. *Chem. Soc. Rev.* **2009**, *38*, 2922–2934.
(14) Vengris, M.; van Stokkum, I. H. M.; He, X.; Bell, A. F.; Tonge, P. J.; van Grondelle, R.; Larsen, D. S. *J. Phys. Chem. A.* **2004**, *108*, 4587–4598.
(15) Niwa, H.; Inouye, S.; Hirano, T.; Matsuno, T.; Kojima, S.; Kubota, M.; Ohashi, M.; Tsuji, F. I. *Proc. Natl. Acad. Sci. U. S. A.* **1996**, *93*, 13617–13622.
(16) Follenius-Wund, A.; Bourotte, M.; Schmitt, M.; Iyice, F.; Lami, H.; Bourguignon, J.-J.; Haiech, J.; Pigault, C. *Biophys. J.* **2003**, *85*, 1839–1850.
(17) (a) Leiderman, P.; Genosar, L.; Huppert, D.; Shu, X.; Remington, S. J.; Solntsev, K. M.; Tolbert, L. M. *Biochemistry* **2007**, *46*, 12026–12036. (b) Kummer, A. D.; Kompa, C.; Lossau, H.; Pöllinger-Dammer, F.; Michel-Beyerle, M. E.; Silva, C. M.; Bylina, E. J.; Coleman, W. J.; Yang, M. M.; Youvan, D. C. *Chem. Phys.* **1998**, *237*, 183–193. (c) Kummer, A. D.; Wiehler, J.; Rehaber, H.; Kompa, C.; Steipe, B.; Michel-Beyerle, M. E. *J. Phys. Chem. B* **2000**, *104*, 4791–4798. (d) Kummer, A. D.; Wiehler, J.; Schüttrigkeit, T. A.; Berger, B. W.; Steipe, B.; Michel-Beyerle, M. E. *Chembiochem* **2002**, *3*, 659–663. (e) Kummer, A. D.; Kompa, C.; Niwa, H.; Hirano, T.; Kojima, S.; Michel-Beyerle, M. E. *J. Phys. Chem. B* **2002**, *106*, 7554–7559. (f) Chen, M. C.; Lambert, C. R.; Urgitis, J. D.; Zimmer, M. *Chem. Phys.* **2001**, *270*, 157–164. (g) Mauring, K.; Krasnenko, V.; Miller, S. *J. Lumin.* **2007**, *122*−*123*, 291–293.
(18) (a) Martin, M. E.; Negri, F.; Olivucci, M. *J. Am. Chem. Soc.* **2004**, *126*, 5452–5464. (b) Rajbongshi, B. K.; Sen, P.; Ramanathan, G. *Chem. Phys. Lett.* **2010**, *494*, 295–300. (c) Stavrov, S. S.; Solntsev, K. M.; Tolbert, L. M.; Huppert, D. *J. Am. Chem. Soc.* **2006**, *128*, 1540–1546.
(19) (a) Gepshtein, R.; Huppert, D.; Agmon, N. *J. Phys. Chem. B* **2006**, *110*, 4434–4442. (b) Altoe, P.; Bernardi, F.; Garavelli, M.; Orlandi, G.; Negri, F. *J. Am. Chem. Soc.* **2005**, *127*, 3952–3963.

(c) Voityuk, A. A.; Michel-Beyerle, M.-E.; Rösch, N. *Chem. Phys. Lett.* **1998**, *296*, 269–276. (d) Yang, J.-S.; Huang, G.-J.; Liu, Y.-H.; Peng, S.-M. *Chem. Commun.* **2008**, 1344–1346. (e) Solntsev, K. M.; Poizat, O.; Dong, J.; Rehault, J.; Lou, Y.; Burda, C.; Tolbert, L. M. *J. Phys. Chem. B* **2008**, *112*, 2700–2711.

(20) (a) Webber, N. M.; Litvinenko, K. L.; Meech, S. R. *J. Phys. Chem. B* **2001**, *105*, 8036–8039. (b) Megley, C. M.; Dickson, L. A.; Maddalo, S. L.; Chandler, G. J.; Zimmer, M. *J. Phys. Chem. B* **2009**, *113*, 302–308. (c) Baffour-Awuah, N. Y. A.; Zimmer, M. *Chem. Phys.* **2004**, *303*, 7–11. (d) Litvinenko, K. L.; Webber, N. M.; Meech, S. R. *Chem. Phys. Lett.* **2001**, *346*, 47–53. (e) Mandal, D.; Tahara, T.; Webber, N. M.; Meech, S. R. *Chem. Phys. Lett.* **2002**, *358*, 495–501. (f) Mandal, D.; Tahara, T.; Meech, S. R. *J. Phys. Chem. B* **2004**, *108*, 1102–1108. (g) Litvinenko, K. L.; Webber, N. M.; Meech, S. R. *J. Phys. Chem. A* **2003**, *107*, 2616–2623. (h) Maddalo, S. L.; Zimmer, M. *Photochem. Photobiol.* **2006**, *82*, 367–372. (i) Litvinenko, K. L.; Webber, N. M.; Meech, S. R. *Bull. Chem. Soc. Jpn.* **2002**, *75*, 1065–1070. (j) Toniolo, A.; Olsen, S.; Manohar, L; Martínez, T. J. *Faraday Discuss.* **2004**, *127*, 149–163.

(21) Weber, W.; Helms, V.; McCammon, J. A.; Langhoff, P. W. *Proc. Natl. Acad. Sci. U.S.A.* **1999**, *96*, 6177–6182.

(22) (a) Branchini, B. R.; Lusins, J. O.; Zimmer, M. *J. Biomol. Struct. Dyn.* **1997**, *14*, 441–448. (b) Voliani, V.; Bizzarri, R.; Nifosì, R.; Abbruzzetti, S.; Grandi, E.; Viappiani, C.; Beltram, F. *J. Phys. Chem. B* **2008**, *112*, 10714–10722. (c) Chen, K.-Y.; Cheng, Y.-M.; Lai, C.-H.; Hsu, C.-C.; Ho, M.-L.; Lee, G.-H.; Chou, P.-T. *J. Am. Chem. Soc.* **2007**, *129*, 4534–4535. (d) Dong, J.; Solntsev, K. M.; Poizat, O.; Tolbert, L. M. *J. Am. Chem. Soc.* **2007**, *129*, 10084–10085. (e) Dong, J.; Solntsev, K. M.; Tolbert, L. M. *J. Am. Chem. Soc.* **2006**, *128*, 12038–12039. (f) Baldridge, A.; Samanta, S. R.; Jayaraj, N.; Ramamurthy, V.; Tolbert, L. M. *J. Am. Chem. Soc.* **2011**, *133*, 712–715. (g) Olsen, S.; Smith, S. C. *J. Am. Chem. Soc.* **2008**, *130*, 8677–8689.

(23) Petkova, I.; Dobrikov, G.; Banerji, N.; Duvanel, G.; Perez, R.; Dimitrov, V.; Nikolov, P.; Vauthey, E. *J. Phys. Chem. A* **2010**, *114*, 10–20.

(24) Baldridge, A.; Samanta, S. R.; Jayaraj, N.; Ramamurthy, V.; Tolbert, L. M. *J. Am. Chem. Soc.* **2010**, *132*, 1498–1499.

(25) Usman, A.; Mohammed, O. F.; Nibbering, E. T. J.; Dong, J.; Solntsev, K. M.; Tolbert, L. M. *J. Am. Chem. Soc.* **2005**, *127*, 11214–11215.

(26) (a) Tolbert, L. M.; Baldridge, A.; Kowalik, J.; Solntsev, K. M. *Acc. Chem. Res.* DOI: 10.1021/ar2000925. (b) Bravaya, K. B.; Grigorenko, B. L.; Nemukhin, A. V.; Krylov, A. A. I. *Acc. Chem. Res.* DOI: 10.1021/ar2001556.

(27) (a) Velsko, S. P.; Fleming, G. R. *Chem. Phys.* **1982**, *65*, 59–70. (b) Duxbury, D. F. *Chem. Rev.* **1993**, *93*, 381–433. (c) Ben-Amotz, D.; Harris, C. B. *J. Chem. Phys.* **1987**, *86*, 4856–4870. (d) Sundström, V.; Gillbro, T.; Bergstörm, H. *Chem. Phys.* **1982**, *73*, 439–458. (e) Rafiq, S.; Yadav, R.; Sen, P. *J. Phys. Chem. B* **2010**, *114*, 13988–13994.

(28) Diwu, Z.; Lu, Y.; Zhang, C.; Klaubert, D. H.; Haugland, R. P. *Photochem. Photobiol.* **1997**, *66*, 424–431.

(29) Rajbongshi, B. K.; Ramanathan, G. *J. Chem. Sci.* **2009**, *121*, 973–982.

(30) Badr, M. Z.; El-Sherief, H. A. H.; Tadros, M. E. *Bull. Chem. Soc. Jpn.* **1982**, *55*, 2267–2270.

(31) Bhattacharjya, G.; Agasti, S. S.; Ramanathan, G. *ARKIVOC* **2006**, *10*, 152–161.

(32) Hoshina, H.; Tsuru, H.; Kubo, K.; Igarashi, T.; Sakurai, T. *Heterocycles* **2000**, *53*, 2261–2274.

(33) Mukerjee, A. K.; Kumar, P. *Heterocycles* **1981**, *16*, 1995–2034.

(34) Sen, P.; Roy, D.; Mondal, S. K.; Sahu, K.; Ghosh, S.; Bhattacharyya, K. *J. Phys. Chem. A* **2005**, *109*, 9716–9722.

(35) (a) Jamorski, C.; Casida, M. E.; Salahub, D. R. *J. Chem. Phys.* **1996**, *104*, 5134–5147. (b) Petersilka, M.; Gossmann, U. J.; Gross, E. K. U. *Phys. Rev. Lett.* **1996**, *76*, 1212–1215. (c) Bauernschmitt, R.; Ahlrichs, R.; Hennrich, F. H.; Kappes, M. M. *J. Am. Chem. Soc.* **1998**, *120*, 5052–5059. (d) Casida, M. E.; Jamorski, C.; Casida, K. C.; Salahub, D. R. *J. Chem. Phys.* **1998**, *108*, 4439–4449. (e) Stratmann, R. E.; Scuseria, G. E.; Frisch, M. J. *J. Chem. Phys.* **1998**, *109*, 8218–8224.

(36) Frisch, M. J.; Trucks, G. W.; Schlegel, H. B.; Scuseria, G. E.; Robb, M. A.; Cheeseman, J. R.; Scalmani, G.; Barone, V.; Mennucci, B.; Petersson, G. A.; Nakatsuji, H.; Caricato, M.; Li, X.; Hratchian, H. P.; Izmaylov, A. F.; Bloino, J.; Zheng, G.; Sonnenberg, J. L.; Hada, M.; Ehara, M.; Toyota, K.; Fukuda, R.; Hasegawa, J.; Ishida, M.; Nakajima, T.; Honda, Y.; Kitao, O.; Nakai, H.; Vreven, T.; Montgomery, J. A. Jr.; Peralta, J. E.; Ogliaro, F.; Bearpark, M.; Heyd, J. J.; Brothers, E.; Kudin, K. N.; Staroverov, V. N.; Kobayashi, R.; Normand, J.; Raghavachari, K.; Rendell, A.; Burant, J. C.; Iyengar, S. S.; Tomasi, J.; Cossi, M.; Rega, N.; Millam, J. M.; Klene,M.; Knox, J. E.; Cross, J. B.; Bakken, V.; Adamo, C.; Jaramillo, J.; Gomperts, R.; Stratmann, R. E.; Yazyev, O.; Austin, A. J.; Cammi, R.; Pomelli, C.; Ochterski, J. W.; Martin, R. L.; Morokuma, K.; Zakrzewski, V. G.; Voth, G. A.; Salvador, P.; Dannenberg, J. J.; Dapprich, S.; Daniels, A. D.; Farkas, O.; Foresman, J. B.; Ortiz, J. V.; Cioslowski, J.; Fox, D. J. *Gaussian 03*, rev C.02; Gaussian, Inc.: Wallingford, CT, 2004.

(37) (a) Lee, C.; Yang, W.; Parr, R. G. *Phys. Rev. B* **1988**, *37*, 785–789. (b) Becke, A. D. *J. Chem. Phys.* **1993**, *98*, 5648–5652.

(38) (a) Autschbach, J. *Chem. Phys. Chem.* **2009**, *10*, 1757–1760. (b) Niehaus, T. A.; March, N. H. *Theor. Chem. Acc.* **2010**, *125*, 427–432. (c) List, N. H.; Olsen J. M.; Rocha-Rinza, T.; Christiansen, O.; Kongsted, J. *Int. J. Quantum Chem.* 2011, published online (DOI: 10.1002/qua.23059).

(39) Kurashige, Y.; Nakajima, T.; Kurashige, S.; Hirao, K. *J. Phys. Chem. A* **2007**, *111*, 5544–5548.

(40) (a) Maroncelli, M.; Fleming, G. R. *J. Chem. Phys.* **1987**, *86*, 6221. (b) Rafiq, S.; Yadav, R.; Sen, P. *J. Phys. Chem A* **2011**, *115*, 8335–8343.

(41) (a) Koti, A. S. R.; Krishna, M. M. G.; Periasamy, N. *J. Phys. Chem. A* **2001**, *105*, 1767–1771. (b) Koti, A. S. R.; Periasamy, N. *Proc. Ind. Acad. Sci.* **2001**, *113*, 157–163. (c) Koti, A. S. R.; Periasamy, N. *J. Chem. Phys.* **2001**, *115*, 7094–7099.

(42) Sherin, P. S.; Grilj, J.; Tsentalovich, Y. P.; Vauthey, E. *J. Phys. Chem. B* **2009**, *113*, 4953–4963.

(43) Fürstenberg, A.; Vauthey, E. *Photochem. Photobiol. Sci.* **2005**, *4*, 260–267.

(44) Nishiya, T.; Yamauchi, S.; Hirota, N.; Baba, M.; Hanazaki, I. *J. Phys. Chem.* **1986**, *90*, 5730–5735.

(45) Levine, B. G.; Martínez, T. J. *Annu. Rev. Phys. Chem.* **2007**, *58*, 613–634.